HEAT AND MASS TRANSPORT OF HYDROMAGNETIC WILLIAMSON NANOFLUID PASSING THROUGH A PERMEABLE MEDIA ACROSS AN EXTENDED SHEET OF VARYING THICKNESS

by

Sanju JANGID[a], Ruchika MEHTA[a*], Jagdev SINGH[b], Dumitru BALEANU[c,d,e], and Ali Saleh ALSHOMRANI[f]

[a] Department of Mathematics and Statistics, Manipal University Jaipur, Jaipur, Rajasthan, India
[b] Department of Mathematics, JECRC University, Jaipur, Jaipur, Rajasthan, India
[c] Department of Mathematics, Faculty of Arts and Sciences, Cankaya University, Etimesgut, Turkey
[d] Institute of Space Sciences, Magurele-Bucharest, Romania
[e] Lebanese American University, Beirut, Lebanon
[f] Mathematical Modelling and Applied Computation (MMAC) Research Group, Department of Mathematics, Faculty of Science, King Abdulaziz University, Jeddah, Saudi Arabia

Original scientific paper
https://doi.org/10.2298/TSCI23S1129J

The primary goal of this work is to determine heat and mass transfer through fluid-flows sheets dealing mathematical modelling for stagnant and varying thickness, considering magnetic fields, permeability, heat source/sink, radiation, Joule heating, chemical reactions, and buoyancy force. The Runge-Kutta fourth order Method (RK-4th order) is used to transform PDE into ODE utilizing similarity conversions. To tabularize mathematical remarks of the local parameters, RK-4th has been developed in MATLAB. For diverse parameters under diverse constant and changing thickness circumstances of fluid characteristics, Nusselt and Sherwood parameters are examined and quantified. Temperature, velocity, and volume fraction graphical representations are used to describe the effects of various factors. When it comes to irregular fluid properties, the coefficient of skin friction has a bigger impact than when it comes to continuous fluid characteristics. However, in the situation of inconstant fluid properties, the local Nusselt number is smaller than in the case of constant fluid characteristics. The RK 4th technique produced high precision computational results, according to the findings.

Key words: *Williamson nanofluid, varying thermal conductivity, varying thickness, RK-4th, buoyancy force*

Introduction

Nanofluid is a new type of fluid created by combining nanometer sized particles with the basic fluids. Because of their superior thermophysical characteristics, the use of nanofluids in place of base fluids has been discovered to have potential utilization in a variety of fields.

Hayat *e al*. [1] examined the impacts of heterogenous and homogenous reactions of various types of base fluid along with nanoparticles passes via a non-linear stretched surface with instable surface profile. Kho *et al.* [2] discussed the heat transport with thermos radiative impression on Williamson fluid over a stretched sheet along with hydromagnetic impact and

* Corresponding author, e-mail: ruchika.mehta1981@gmail.com

nanoparticles. Krishna *et al.* [3] analyze 3-D nanofluid motion under the impact of slip effect and heat radiation on a non-uniform thickness mounting sheet using Cu-water and $Al_{50}Cu_{50}$-water nanofluids. The impacts of non-linear thermal radiation and 1st order chemical reaction on the boundary-layer flow of Williamson nanofluid across a non-uniformly thicked stretched Riga plate were explored by Kumar *et al.* [4]. Reddy *et al.* [5] considered the velocity and heat transfer profiles along with the variable thickness and thermal conductivity of non-Newtonian Williamson fluid with nanoparticles. Hamid and Khan [6] examined the unsteady flow of Williamson nanofluid pushed by a radially extending geometry under the impact of a moving magnetic field, mixed convection, and the newly suggested zero nanoparticles mass flux assumption.

Aliy and Kishan [7] analyzed the electromagnetism flow of Williamson nanofluid with heat and mass transference over a warmed non-flat surface along with a varying thickness under the influence of an electric field. Kumar *et al.* [8] researched the heat and mass transport appearances of 3-D bio convective nanofluid-flow across a slandering surface with slip impacts under uneven heat sink or source, the rmophoresis, and Brownian motion of nanoparticles. Ramzan *et al.* [9] deliberated the 2nd-order slipping and dual segmentation coatings on non-Newtonian Williamson fluid with nanoparticles along with MHD impression and Cattaneo-Christov heat flux. Shawky *et al.* [10] considered the fluid-flow and heat transport of hydromagnetic Williamson with nanoparticles over the stretched surface in the porous medium. In the existence of thermal radiative impression, heat source, and varying permeability, Ibrahim and Gamachu [11] examined a non-linear convection flow of Williamson nanofluidover a radially stretched surface under the impact of an electric field. Amer Qureshi [12] discussed the heat transport and fluid-flow of hydromagnetic Williamson fluid in the existence of nanosized particles along with thermal radiative impact. A study of Williamson fluid with nanosized particles passes through a stretched sheet along with the constant and inconstant thickness and the hydromagnetic impact was studied by Sridhar *et al.* [13]. In the existence of non-linear thermal radiative, activation energy, motile microorganisms, thermophoresis, and Brownian motion, Kumaran and Sivaraj [14] explored the hydromagnetic Williamson nanofluid Falkner-Skan flow across a wedge/flat plate/stagnation point. Srinivasulu and Goud [15] considered the impression of the inclined magnetic field with the impacts of heat mass transport of Williamson fluid in the presence of nanoparticles over a stretched surface.

Williamson nanofluid-flow over extending sheet with constant and inconstant widths has been researched in existing work with new result of [13], which includes magnetic fields, electric fields, porous enclosed space, heat propagation/absorption, and radiative heat propagation using the RK-4th order method. The data is displayed as movement, temperature, and volume fraction profiles.

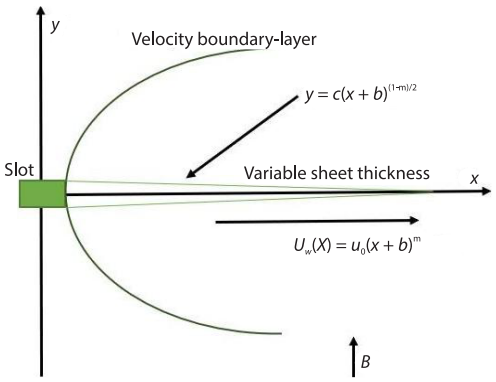

Figure 1. Flow structure of the existing research

Methodology

Figure 1 shows a schematic representation of the physical system. On a stretched horizontal sheet, a 2-D time-independent hydromagnetic Williamson nanofluid is studied. The origin is established at the spot where the sheet is taken in the fluid transportable region. The velocity of the stretched sheet is $U_w = u_0(x + b)^m$. For diverse applications, by reason of the acceleration or deceleration of the sheet, the width of the stretching sheet may reduction or upsurge with detachment from the slot, which is

reliant on the cost of the momentum power index parameter, m. For $m = 1$, the sheet is flat. The stretched sheet is considered along the x, y-axis, which is parallel to the stretching sheet. Consider that the width of the sheet varies according to the relationship $y = c(x + b)^{(1-m)^2}$. Constants c and b is used here. The magnetic field is tailored to the flow of nanofluids in a transverse direction. The induced magnetic field is negligible when compared to the applied magnetic field.

Constitutional relations for non-Newtonian Williamson fluid are [2, 7, 12]:

$$S = -PI + \tau, \ \ \tau = \left(\mu_\infty + \frac{\mu_0 - \mu_\infty}{1 - \Gamma\gamma} \right) A_1 \tag{1}$$

where P is the view points for pressure, I – the display for identity vector, τ – the proposals the extra stress tensor, μ_0 and μ_∞ – the exhibition for limit viscidness at 0, and ∞ – the shear rate, respectively, A_1 shows the Rivilin-Erickson tensor and γ defined:

$$\gamma = \sqrt{\frac{1}{2}\pi}, \ \ \pi = \text{trace}\left(A_1\right)^2 \tag{2}$$

The dimensional governing relations of current work are emblazoned as tracks [6, 13]:

$$\frac{\partial u}{\partial x} + \frac{\partial v}{\partial y} = 0 \tag{3}$$

$$u\frac{\partial u}{\partial x} + v\frac{\partial u}{\partial y} = \nu\frac{\partial^2 u}{\partial y^2} + \sqrt{2}\,\Gamma\nu\frac{\partial u}{\partial y}\frac{\partial^2 u}{\partial y^2} - \frac{\sigma B^2 u}{\rho} - \frac{\nu u}{k'} + g_0\beta_T\left(T - T_\infty\right) + g_0\beta_C\left(C - C_\infty\right) \tag{4}$$

$$u\frac{\partial T}{\partial x} + v\frac{\partial T}{\partial y} = \frac{1}{\rho C_p}\frac{\partial}{\partial y}\left(k\frac{\partial T}{\partial y}\right) + \frac{(\rho c)_p}{(\rho c)_f} \cdot$$
$$\cdot\left[\frac{D_T}{T_\infty}\left(\frac{\partial T}{\partial y}\right)^2 + D_B\left(\frac{\partial T}{\partial y}\frac{\partial C}{\partial y}\right)\right] - \frac{1}{\rho C_p}\frac{\partial q_r}{\partial y} + \frac{\sigma B^2 u^2}{\rho C_p} + \frac{Q_0}{\rho C_p}\left(T - T_\infty\right) \tag{5}$$

$$u\frac{\partial C}{\partial x} + v\frac{\partial C}{\partial y} = D_B\frac{\partial^2 C}{\partial y^2} + \frac{D_T}{T_\infty}\frac{\partial^2 T}{\partial y^2} - R^*\left(C - C_\infty\right) \tag{6}$$

The associatory limitations [13]:

$$\begin{gathered} u = U_w\left(x\right) = u_0\left(x + b\right)^m \ \ v = 0, \ T = T_w, \ C = C_w, \ \text{at} \ \ y = c\left(x + b\right)^{(1-m)/2} \\ u = 0, \ T = T_\infty, \ C = C_\infty, \ \text{at} \ \ y \to \infty \end{gathered} \tag{7}$$

where u [ms^{-1}] and v [ms^{-1}] are the designate the x-axis and y-axis momentum components, respectively, T – the positions for the temperature, C – the positions for the volume fraction, Γ stands for the $^{+ve}$ time constant, ν [m^{-2}s^{-1}] – the kinematic viscosity, σ – the conductivity electricity field, ρ – the fluid density, the thermophoresis and Brownian diffusions coefficients are shortest by D_T [m^{-2}s^{-1}] and D_B [m^{-2}s^{-1}], Q – the dimensional heat source or sink coefficient, k [m^{-2}s^{-1}] – the thermal conductivity, C_p – the specific heat, u_0 – the rate of stretched surface, B [NmA^{-1}] – the magneto field strength, T_∞ and C_∞ – the position for the ambient temperature and ambient volume fraction of nanoparticles, $(\rho c)_p$ – the heat capacity of nanoparticles, $(\rho c)_p$ [Jm^{-3}K^{-1}] – the heat capacity of nanofluids, and w and ∞ indicate to the condition at surface and the free stream.

The Roseland approximation of the radiative heat flux is settled:

$$q_r = \frac{-4\sigma^*}{3k^*}\frac{\partial T^4}{\partial y} \tag{8}$$

where T^4 as a linear relation of temperature via Taylor's sequence expansion about T_∞ and ignoring advanced terms:

$$T^4 \approx 4T_\infty^3 T - T_\infty^4 \tag{9}$$

With the procedure of the under-mentioned similarity transformations:

$$\eta = \sqrt{\frac{u_0(1+m)}{2\nu}}\left(y(x+b)^{(m-1)/2} - c\right),\ \psi = \sqrt{\frac{u_0 2\nu}{(1+m)}}(x+b)^{(m+1)/2} f$$

$$u = \frac{\partial \psi}{\partial y} = u_0(x+b)^m f'(\eta)$$

$$v = -\frac{\partial \psi}{\partial x} = -u_0(x+b)^{(m-1)/2}\frac{(m-1)}{2} f'\left\{\eta\sqrt{\frac{2\nu}{u_0(1+m)}} + c\right\} - \sqrt{\frac{u_0 2\nu}{(1+m)}}(x+b)^{(m+1)/2}\frac{(m+1)}{2} \tag{10}$$

$$\theta(\eta) = \frac{T - T_\infty}{T_w - T_\infty},\ \phi(\eta) = \frac{C - C_\infty}{C_w - C_\infty}$$

With the help of aforementioned similarity transformations eq. (10) in eq. (1) to eq. (6) along with eqs. (7)-(9), the under-mentioned dimensionless equations:

$$f''' = \frac{\left\{\frac{2m}{(m+1)}(f')^2 - ff'' + \mathrm{Mn}f' + k_2 f' - G_T\theta - G_C\phi\right\}}{(1+Wf'')} \tag{11}$$

$$\theta'' = (-1)\mathrm{Pr}\frac{\left\{f\theta' + Nb\theta'\phi' + Nt(\theta')^2 + \mathrm{MnEc}(f')^2 + Q\theta\right\}}{(1+Nr)} \tag{12}$$

$$\phi'' = \mathrm{Sc}K\phi - \mathrm{Sc}f\phi' - \left(\frac{Nt}{Nb}\right)\theta'' \tag{13}$$

and limitations are specified:

$$f(0) = a\frac{(1-m)}{(1+m)},\ f'(0) = 1,\ \theta(0) = 1,\ \phi(0) = 1,\ \text{at}\ \ \eta = 0$$
$$f'(\infty) \to 0,\ \theta(\infty) \to 0,\ \phi(\infty) \to 0,\ \text{at}\ \ \eta \to \infty \tag{14}$$

where

$$W = \Gamma\sqrt{\frac{{U_0}^3(1+m)(x+b)^{3m-1}}{\nu}}$$

describes the dimensionless Weissenberg parameter

$$Mn = \frac{2\sigma B^2}{\rho u_0(1+m)(x+b)^{m-1}}$$

exhibits the magnetic (Hartman) parameter

$$k_2 = \frac{2\nu}{k' u_0 \left(1+m\right)\left(x+b\right)^{m-1}}$$

defines the permeability parameter

$$G_T = \frac{2g_0\beta_T\left(T_w - T_\infty\right)}{{u_0}^2\left(1+m\right)\left(x+b\right)^{2m-1}}, \text{ and } G_C = \frac{2g_0\beta_c\left(C_w - C_\infty\right)}{{u_0}^2\left(1+m\right)\left(x+b\right)^{2m-1}}$$

describes the local temperature and volume fraction Grashof number, respectively

$$Nr = \frac{16\sigma^* T_\infty^3}{3kk^*}$$

shows the radiative impression

$$\Pr = \frac{\mu C_p}{k}$$

depicts the Prandtl number

$$Q = \frac{2Q_0}{C_p \rho u_0 \left(1+m\right)\left(x+b\right)^{m-1}}$$

shows the heat source or sink parameter

$$Nb = \frac{(\rho c)_p}{(\rho c)_f}\frac{D_B\left(C_w - C_\infty\right)}{\nu}$$

depicts the Brownian motion parameter

$$Nt = \frac{(\rho c)_p}{(\rho c)_f}\frac{D_T\left(T_w - T_\infty\right)}{\nu T_\infty}$$

depicts the thermophoresis diffusion influence

$$\mathrm{Ec} = \frac{{u_0}^2\left(x+b\right)^{2m}}{C_p\left(T_w - T_\infty\right)}$$

exhibits the Eckert parameter

$$\mathrm{Sc} = \frac{\nu}{D_B}$$

shows the Schmidt number

$$K = \frac{R^*}{u_0\left(1+m\right)\left(x+b\right)^{m-1}}$$

depicts the chemically reactive number, and

$$a = c\sqrt{\frac{u_0\left(1+m\right)}{2\nu}}$$

depicts a parameter connected to the width of the wall (called the wall thickness parameter).

Friction factor, C_{fx}, local Nusselt number, Nu_x, and Sherwood number, Sh_x, are some additional important physical variables. These are described:

$$C_{f_x} = \frac{2\tau_w}{\rho U_w^2} = (1+m)\,\mathrm{Re}_x^{-1/2} f''(0), \text{ where } \tau_w = \mu\left(\frac{\partial u}{\partial y}\right)_{y=c(x+b)^{(1-m)/2}} \tag{15}$$

$$\mathrm{Nu}_x = \frac{xq_w}{k(T_w - T_\infty)} = -\mathrm{Re}_x^{1/2}\theta'(0), \text{ where } q_w = -k\left(\frac{\partial T}{\partial y}\right)_{y=c(x+b)^{(1-m)/2}} \tag{16}$$

$$\mathrm{Sh}_x = \frac{xp_w}{D_B(C_\mathrm{w} - C_\infty)} = -\mathrm{Re}_x^{1/2}\phi'(0), \text{ where } p_w = -D_B\left(\frac{\partial C}{\partial y}\right)_{y=c(x+b)^{(1-m)/2}} \tag{17}$$

where

$$\mathrm{Re}_x = \frac{u_0(1+m)(x+b)^{(1+m)}}{2\nu}$$

is the Reynolds number.

Numerical structure

Equations are solved via RK-4th order technique and shooting method. All numerical values and graphs are found with MATLAB software which is discussed in through tables and graphs. First, apply the shooting method:

$$f = f_1,\ f' = f_2,\ f'' = f_3,\ \theta = f_4,\ \theta' = f_5,\ \phi = f_6,\ \phi' = f_7$$

Equations (11)-(14) reduce into new form:

$$f''' = \frac{\left\{\frac{2m}{(m+1)}(f_2)^2 - f_1 f_3 + \mathrm{Mn} f_2 + k_2 f_2 - G_T f_4 - G_C f_6\right\}}{(1+Wf_3)} \tag{18}$$

$$\theta'' = (-1)\,\mathrm{Pr}\frac{\left\{f_1 f_5 + Nbf_5 f_7 + Nt(f_5)^2 + \mathrm{MnEc}(f_2)^2 + Qf_4\right\}}{(1+Nr)} \tag{19}$$

$$\phi'' = \mathrm{Sc}Kf_6 - \mathrm{Sc}ff_7 - \left(\frac{Nt}{Nb}\right)\theta'' \tag{20}$$

and limitations are specified:

$$\begin{gathered} f_1 = a\frac{(1-m)}{(1+m)},\ f_2 = 1,\ f_4 = 1,\ f_6 = 1,\ \text{at}\ \ \eta = 0 \\ f_2 \to 0,\ f_4 \to 0,\ f_6 \to 0,\ \text{at}\ \ \eta \to \infty \end{gathered} \tag{21}$$

Numerical result and discussion

The Runge-Kutta approach is used to evaluate the mathematical results of Williamson nanofluid atop an extending sheet with uneven thickness and uneven thermal conductivity. The findings are consistent with earlier research. The current findings are found to be very consis-

tent with past research. Figures 2-32 and tabs. 1 and 2 illustrate the influence of several physical parameter values on momentum, temperature, volume fraction, skin-friction coefficient, Nusselt number, and Sherwood number values developed with MATLAB software.

For current research, we measured the values of physical parameters as: $W = 0.1 = k_2 = G_T = G_C = Nr = Nb = Nt = \text{Ec} = Q$, $\text{Mn} = \text{Sc} = a = m = 0.5$, $\text{Pr} = 0.7$, and $K = 0.6$. Figure 2 shows the impact of the upsurge W on momentum profile. Because the Williamson parameter causes more restriction in fluid-flow, momentum declines when the elasticity stress parameter improves. Figures 3 and 11 depict the growing impression of the Mn on the momentum and the temperature profiles, respectively. By reason of an opposite force known as the Lorentz force, velocity graphs are found to be reduced when Hartman parameter values are improved. The temperature outline shows an increasing trend because, when Mn levels rise, fluid particle mobility ceases and diffuses swiftly to the boundary's adjoining layers. The improving permeability parameter k_2 declines the velocity profile and improves the temperature profile in figs. 4 and 12, respectively. Figures 5 and 13 show the growing momentum profile and the falling temperature profile impressions of the upsurge local temperature G_T. Similarly, we see the increasing local concentration G_C, impression in figs. 6 and 14. Because the Grash of number is

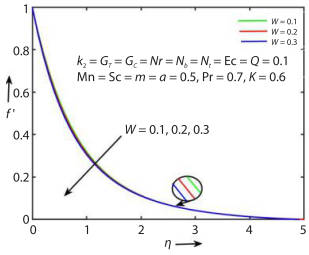

Figure 2. Momentum drawings for numerous W values

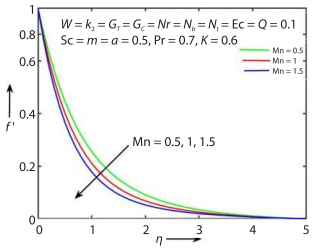

Figure 3. Momentum drawings for numerous Mn values

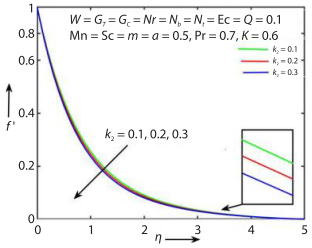

Figure 4. Momentum drawings for numerous k_2 values

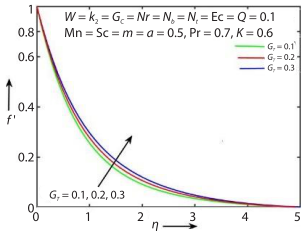

Figure 5. Momentum drawings for numerous G_T values

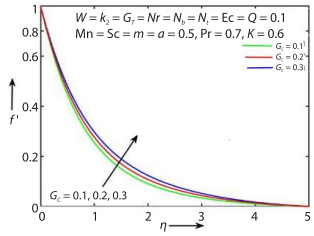

Figure 6. Momentum drawings for numerous G_C values

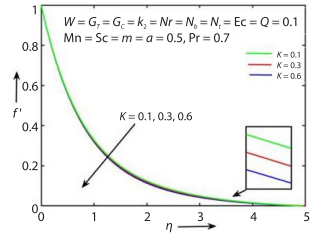

Figure 7. Momentum drawings for numerous K values

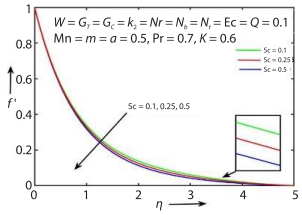

Figure 8. Momentum drawings for numerous Sc values

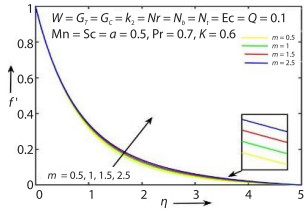

Figure 9. Momentum drawings for numerous m values

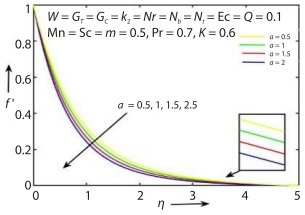

Figure 10. Momentum drawings for numerous a value

the fraction of buoyancy to restraining force. The buoyant force is caused by the spatial difference in fluid density and the restraining force caused by the fluid's viscosity.

Figures 7 and 24 depict the decreasing momentum and volume fraction profiles of the rising chemical reaction parameter. An increasing impression of Schmidt number, is shown in figs. 8 and 30, for momentum and concentration outlines, respectively. As the Schmidt number increased, the molecular diffusion coefficient decreased. Figures 9, 21, and 31 illustrate the increasing impact of velocity power index parameter on momentum, temperature and volume fraction profiles, respectively. The thickness of the momentum and heat boundary-layers decreases when the velocity index parameter is increased. Temperature and velocity profiles all show an upward trend because of this impact. Figures 10, 22, and 32 depict the momentum, temperature, and volume fraction profile for the increasing wall thickness parameter. With the upsurge wall thickness parameter the concentration outlines show the rising impact for $\eta < 1.5$ and growing impact for $\eta > 1.5$. When the wall width parameter is increased, velocity and temperature decrease. This occurs because the boundary-layer width becomes narrower when the wall width parameter is enhanced.

The increasing Eckert number, declines the volume fraction profiles and increases the temperature profiles which is shown in figs. 15 and 23. It has been found that when the Eck-

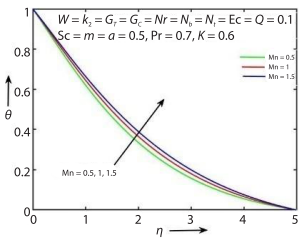

Figure 11. Temperature drawings for numerous Mn values

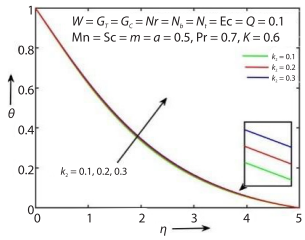

Figure 12. Temperature drawings for numerous k_2 values

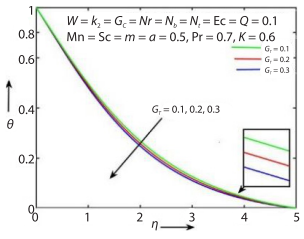

Figure 13. Temperature drawings for numerous G_T values

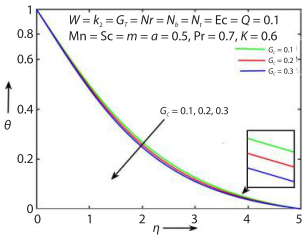

Figure 14. Temperature drawings for numerous G_C values

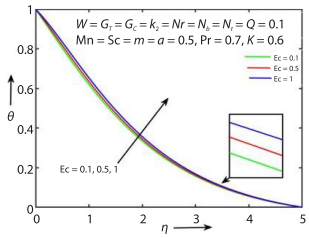

Figure 15. Temperature drawings for numerous Ec values

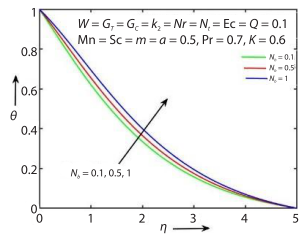

Figure 16. Temperature drawings for numerous *Nb* values

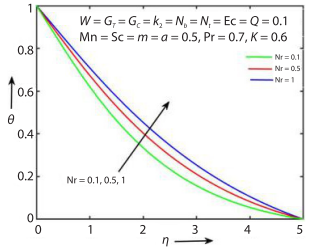

Figure 17. Temperature drawings for numerous *Nb* values

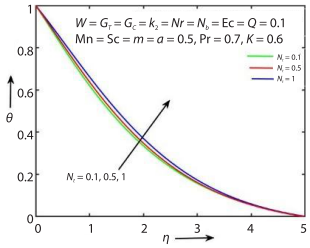

Figure 18. Temperature drawings for numerous *Nt* values

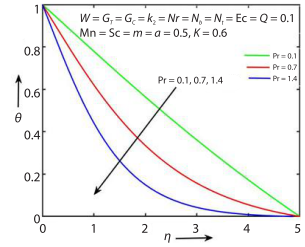

Figure 19. Temperature drawings for numerous Pr values

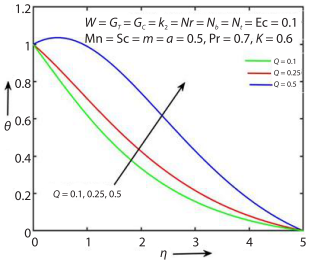

Figure 20. Temperature drawings for numerous *Q* values

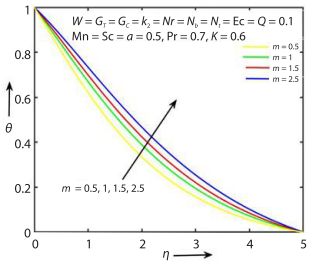

Figure 21. Temperature drawings for numerous *m* values

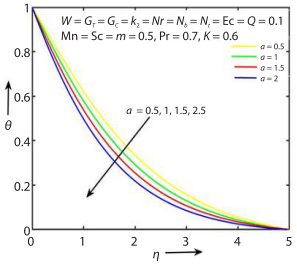

Figure 22. Temperature drawings for numerous *Nb* values

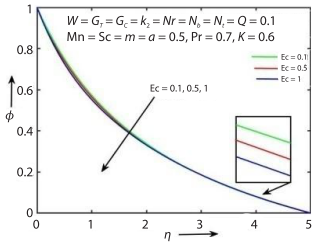

Figure 23. Volume fraction drawings for numerous Ec values

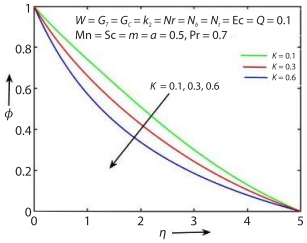

Figure 24. Volume fraction drawings for numerous *K* values

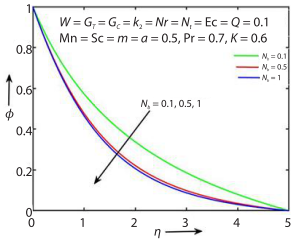

Figure 25. Volume fraction drawings for numerous *Nb* values

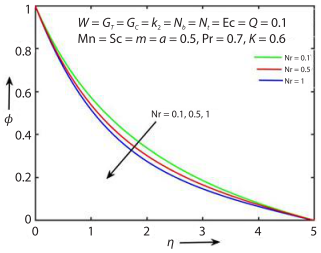

Figure 26. Volume fraction drawings for numerous *Nr* values

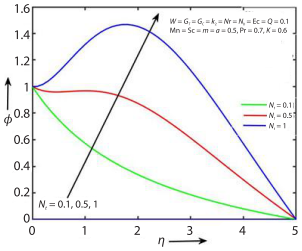

Figure 27. Volume fraction drawings for numerous *Nt* values

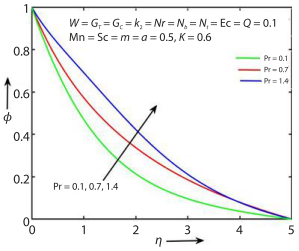

Figure 28. Volume fraction drawings for numerous Pr values

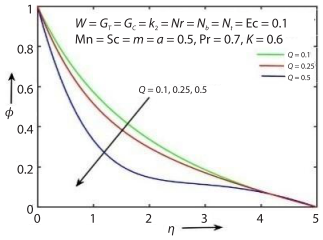

Figure 29. Volume fraction drawings for numerous *Q* values

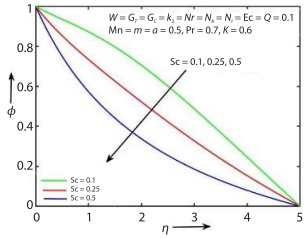

Figure 30. Volume fraction drawings for numerous Sc values

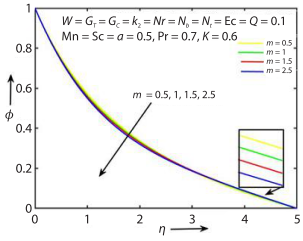

Figure 31. Volume fraction drawings for numerous *m* values

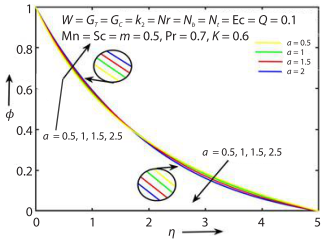

Figure 32. Volume fraction drawings for numerous *a* values (*for color image see journal web site*)

ert number rises, the temperature profile rises as well. The Eckert number labels the connection between kinetic energy and enthalpy in a flow. It represents the labour done in contradiction of viscous fluid forces to renovate kinetic energy into internal energy. A growth in the Eckert number designates that the kinetic energy of the fluid is high, resulting in higher fluid vibration and more fluid-molecule collisions. Augmented molecule collisions promote heat dissipation in the boundary-layer area, subsequent in a rise in temperature profile. The Brownian motion parameter raises the temperature profile, as shown in fig. 16. The reason for this is that various nanoparticles have varying Brownian motion parameters, which causes the heat transport rate to increase. The Brownian motion parameter reduces the concentration profile, as shown in fig. 25.

The growing thermal radiation parameter's upsurge temperature graph and falls volume fraction graph are shown in figs. 17 and 26, respectively. Temperature rises because when *Nr* rises, the thermal boundary-layer rises with it. The increasing thermophoresis diffusion parameter *Nt* increases the temperature profile and volume fraction profile both as shown in figs. 18 and 27. The influence of *Nt* on θ is seen in fig. 18. Tiny fluid particles are pushed back from the warmer to the cold surface in the thermophoresis phenomena. As a result, the fluid particles in the warmed surface returned, and the thermal curve rose. Temperature and concentration patterns for Prandtl number are shown in figs. 19 and 28. The heat conductivity of the fluid decreases as the Prandtl number rises, causing a declination in the thermal profile. In figs. 20 and 29, the impact of the heat source parameter *Q* on θ is shown. The heat

Table 1. The skin-friction coefficient, heat transfer coefficient, and mass transfer coefficient values with respect to some physical parameters *W*, Mn, k_2, G_T, G_C, *Nr*, Pr and *Nb* when *Nt* = Ec = *Q* = 0.1, Sc = *m* = *a* = 0.5 and *K* = 0.6

W	Mn	k_2	G_T	G_C	*Nr*	Pr	*Nb*	$f'(0)$	$-\theta'(0)$	$-\phi'(0)$
0.1								–1.1807	–0.3847	–0.5943
0.2	0.5	0.1	0.1	0.1	0.1	0.7	0.1	–1.2392	–0.3817	–0.5950
0.3								–1.3182	–0.3780	–0.5959
	0.5							–1.1807	–0.3847	–0.5943
0.1	**1**	0.1	0.1	0.1	0.1	0.7	0.1	–1.40912	–0.34955	–0.6114
	1.5							–1.61142	–0.3215	–0.6256
		0.1						–1.1807	–0.3847	–0.5943
0.1	0.5	**0.2**	0.1	0.1	0.1	0.7	0.1	–1.2290	–0.3790	–0.5959
		0.3						–1.2759	–0.3745	–0.5972
			0.1					–1.1807	–0.3847	–0.5943
0.1	0.5	0.1	**0.2**	0.1	0.1	0.7	0.1	–1.1106	–0.3960	–0.5911
			0.3					–1.0429	–0.4065	–0.5879
				0.1				–1.1807	–0.3847	–0.5943
0.1	0.5	0.1	0.1	**0.2**	0.1	0.7	0.1	–1.1121	–0.3960	–0.5911
				0.3				–1.0444	–0.4065	–0.5880
					0.1			–1.1807	–0.3847	–0.5943
0.1	0.5	0.1	0.1	0.1	**0.5**	0.7	0.1	–1.1787	–0.3259	–0.6365
					1			–1.1772	–0.2885	–0.6628
						0.1		–1.1742	–0.2188	–0.7096
0.1	0.5	0.1	0.1	0.1	0.1	**0.7**	0.1	–1.1807	–0.3847	–0.5943
						1.4		–1.1869	–0.6120	–0.4219
							0.1	–1.1807	–0.3847	–0.5943
0.1	0.5	0.1	0.1	0.1	0.1	0.7	**0.5**	–1.1862	–0.3198	–0.7054
							1	–1.1842	–0.2519	–0.7183

source/sink performs the function of a heat generator. The temperature of the fluid particles rises as the parameter estimations get more intense. As a result, there temperature upsurges. As a result, the concentration graph begins to fall.

Table 2. The skin-friction coefficient, heat transfer coefficient, and mass transfer coefficient values with respect to some physical parameters *Nt*, Ec, *Q*, Sc, *m*, *a*, and *K* when $W = k_2 = G_T = G_C = Nr = Nt = 0.1$, Mn = 0.5, and Pr = 0.7

Nt	Ec	*Q*	Sc	*K*	*m*	*a*	$f''(0)$	$-\theta'(0)$	$-\phi'(0)$
0.1							–1.1807	–0.3847	–0.5943
0.5	0.1	0.1	0.5	0.6	0.5	0.5	–1.1446	–0.3535	–0.2266
1							–1.1103	–0.3141	–0.0518
	0.1						–1.1807	–0.3847	–0.5943
0.1	**0.5**	0.1	0.5	0.6	0.5	0.5	–1.1803	–0.3347	–0.6390
	1						–1.1797	–0.2717	–0.6955
		0.1					–1.1807	–0.3847	–0.5943
0.1	0.1	**0.25**	0.5	0.6	0.5	0.5	–1.1776	–0.2417	–0.7092
		0.5					–1.1676	0.1617	–1.0230
			0.1				–1.1550	–0.4002	–0.1482
0.1	0.1	0.1	**0.25**	0.6	0.5	0.5	–1.1672	–0.3930	–0.3399
			0.5				–1.1807	–0.3847	–0.5943
				0.1			–1.1674	–0.3918	–0.3010
0.1	0.1	0.1	0.5	**0.3**	0.5	0.5	–1.1737	–0.3890	–0.4345
				0.6			–1.1807	–0.3847	–0.5943
					0.5		–1.1807	–0.3847	–0.5943
0.1	0.1	0.1	0.5	0.6	**1**	0.5	–1.1908	–0.3127	–0.6080
					1.5		–1.1986	–0.2718	–0.6130
					2.5		–1.20875	–0.2271	–0.6161
						0.5	–1.1807	–0.3847	–0.5943
0.1	0.1	0.1	0.5	0.6	0.5	**1**	–1.2818	–0.4550	–0.5767
						1.5	–1.3908	–0.5282	–0.5555
						2	–1.5087	–0.6073	–0.5287

Also, comparison of current work with various research work is shown in tab. 3 along with the switch off to new parameters:

Table 3. Validation remarks of -*f*"(0) for *m* amounts when *a* = 0.5, Mn = 0 = *W*

m	[6]	[3]	[13]	Existing work
0	0.9576	0.9577	0.95764824	0.9577
0.5	0.9799	0.9798	0.97994720	0.9799
2	1.0234	1.0234	1.02340525	1.023499
5	1.0486	1.0486	1.04860614	1.0488
9	1.0589	1.0588	1.05890951	1.0591
10	1.0603	1.0603	1.06031823	1.0605

Conclusions

Williamson nanofluid-flow on an extending sheet with uneven thickness and uneven thermal conductivity was investigated in this research. The governing equations were solved

using the RK-4th order method. The under-mentioned conclusions may be drawn from the diagrams are as follows.

- The skin-friction coefficient grows with the increasing physical parameters G_T, G_C, *Nr*, *Nt*, Ec, and *Q* while the opposite impression shows with the increasing *W*, Mn, k_2, *Pr*, Sc, *m*, *a*, *K*, and *Nb*.
- The heat transfer coefficient (Nusselt number) raises with the growing physical parameters *W*, Mn, k_2, *Nr*, *Nt*, Ec, Sc, *m*, *K*, *Nb*, and *Q* while the reverse impress displays with the growing G_T, G_C, a, and Pr.
- The mass transfer coefficient (Sherwood number) promotions with the growing physical parameters G_T, G_C, Pr, *a*, and *Nt* while the differing imprint expressions with the growing *W*, Mn, k_2, *Nr*, Ec, Sc, *m*, *K*, and *Nb*.

References

[1] Hayat, T., *et al*., Effects of Homogeneous and Heterogeneous Reactions in Flow of Nanofluids over a Non-Linear Stretching Surface with Variable Surface Thickness, *Journal of Molecular Liquids*, *221* (2016), Sept., pp. 1121-1127
[2] Kho, Y. B., *et al*., Thermal Radiation Effect on MHD Flow and Heat Transfer Analysis of Williamson Nanofluid Past over a Stretching Sheet with Constant Wall Temperature, *Journal of Physics: Conference Series*, *890* (2017), 1, 012034
[3] Krishna, P. M., *et al*., Thermal Radiation Effect on 3-D Slip Motion of AlCu-Water and Cu-Water Nanofluids over a Variable Thickness Stretched Surface, *Defect and Diffusion Forum*, *377* (2017), Sept., pp. 141-154
[4] Kumar, R., *et al*., Radiative Heat Transfer Study for Flow of Non-Newtonian Nanofluid Past a Riga Plate with Variable Thickness, *Journal of Molecular Liquids*, *248* (2017), Dec., pp. 143-152
[5] Reddy, S., *et al*., The MHD Flow and Heat Transfer Characteristics of Williamson Nanofluid over a Stretching Sheet with Variable Thickness and Variable Thermal Conductivity, Transactions of A, *Razmadze Mathematical Institute*, *171* (2017), 2, pp. 195-211
[6] Hamid, A., Khan, M., Unsteady Mixed Convective Flow of Williamson Nanofluid with Heat Transfer in the Presence of Variable Thermal Conductivity and Magnetic Field, *Journal of Molecular Liquids*, 260 (2018), June, pp. 436-446
[7] Aliy, G., Kishan, N., Effect of Electric Field on MHD Flow and Heat Transfer Characteristics of Williamson Nanofluid over a Heated Surface with Variable Thickness, OHAM Solution, *Journal of Advances in Mathematics and Computer Science*, *30* (2019), 1, pp. 1-23
[8] Kumar, A., *et al*., Impact of Brownian Motion and Thermophoresis on Bioconvective Flow of Nanoliquids Past a Variable Thickness Surface with Slip Effects, *Multidiscipline Modelling in Materials and Structures*, *15* (2019), 1, pp. 103-132
[9] Ramzan, M., *et al.*, Impact of Second-Order Slip and Double Stratification Coatings on 3-D MHD Williamson Nanofluid-Flow with Cattaneo-Christov Heat Flux, *Coatings*, *9* (2019), 12, 849
[10] Shawky, H. M., *et al*., MHD flow with heat and mass transfer of Williamson nanofluid over stretching sheet through porous medium, *Microsystem Technologies*, *25* (2019), 4, pp. 1155-1169
[11] Ibrahim, W., Gamachu, D., Finite Element Method Solution of Mixed Convection Flow of Williamson Nanofluid Past a Radially Stretching Sheet, *Heat Transfer*, *49* (2020), 2, pp. 800-822
[12] Amer Qureshi, M., Numerical Simulation of Heat Transfer Flow Subject to MHD of Williamson Nanofluid with Thermal Radiation, *Symmetry*, *13* (2021), 1, 10
[13] Sridhar, W., *et al*., The MHD Williamson Nanofluid Across a Permeable Medium Past an Extended Sheet with Constant and Irregular Thickness, *Heat Transfer*, *50* (2021), 8, pp. 8134-8154
[14] Kumaran, G., Sivaraj, R., Non-Linear Thermal Radiation Effect on Magnetohydrodynamic Williamson Nanofluid Past a Wedge/Flat Plate/Stagnation Point of the Plate with Activation Energy, *Computational Thermal Sciences: An International Journal*, *13* (2021), 5
[15] Srinivasulu, T., Goud, B. S., Effect of Inclined Magnetic Field on Flow, Heat, and Mass Transfer of Williamson Nanofluid over a Stretching Sheet, *Case Studies in Thermal Engineering*, *23* (2021), 23, 100819

Paper submitted: February 12, 2022
Paper revised: March 14, 2022
Paper accepted: March 24, 2022